J|A|C|S
ARTICLES
Published on Web 06/12/2004

Supramolecular Polymerization and Gel Formation of Bis(Merocyanine) Dyes Driven by Dipolar Aggregation

Sheng Yao,[†] Uwe Beginn,*[,‡] Tobias Gress,[†] Marina Lysetska,[†] and Frank Würthner*[,†]

Contribution from the Institut für Organische Chemie, Universität Würzburg, Am Hubland, D-97070 Würzburg, Germany, and DWI/ITMC - Lehrstuhl für Textilchemie und Makromolekulare Chemie, RWTH-Aachen, Worringerweg 1, D-52056 Aachen, Germany

Received January 21, 2004; E-mail: wuerthner@chemie.uni-wuerzburg.de; uwe.beginn@texmc.rwth-aachen.de

Abstract: Two highly dipolar merocyanine dyes were tethered by a rigid tris(*n*-dodecyloxy)xylylene unit that preorganizes the dyes for a supramolecular polymerization process through intermolecular aggregation of the dyes. UV/vis spectroscopy revealed a solvent dependent equilibrium between monomeric dyes and two different types of dye aggregates that are characterized by hypsochromically shifted *D*- and *H*-type absorption bands. Taking into account the ditopic nature of the supramolecular building blocks, the occurrence of the *D*-band indicates the formation of an oligomeric/polymeric supramolecular chain whereas the observation of the *H*-band suggests a higher order assembly. For the *H*-aggregated dyes, intrinsic viscosities exceed 0.65 L g^{-1} in methylcyclohexane, values typically found for macromolecular solutions. At higher concentration, further association of these aggregates takes place by entanglement of the alkyl groups leading to a substantial increase in viscosity and gelation. Rheology studies show linear viscoelastic behavior which was attributed to the formation of an entangled dynamic network. AFM and cryo-TEM studies of the gel reveal long and stiff rod-type assemblies. X-ray diffraction studies for a solid film show columnar mesomorphism. Based on these results, a structural model is proposed in which six helically preorganized strands of the supramolecular polymer intertwine to form a rod with a diameter of about 5 nm. Within these rods all dyes are tightly aggregated in a tubular fashion giving rise to delocalized excitonic states, and the π-conjugated tube is jacketed by the tridodecyloxy groups.

Introduction

Dye assemblies offer important functionality in nature and technology. Prominent examples from nature are the efficient light harvesting dye aggregates found in purple bacteria[1] and in green bacteria.[2] The latter are especially remarkable as they are composed solely of chlorin dyes (the main component being bacteriochlorophyll c) that self-assemble into extended rod aggregates called chlorosomes. Within these rod aggregates the dyes are packed in a cylindrical fashion by means of coordinative, hydrogen bonding and $\pi-\pi$-stacking noncovalent interactions.[2] If such control of dye−dye aggregate formation could be realized in artificial systems, very interesting properties might arise which will open new avenues for electronic and photonic materials. However, rational control of dye−dye interactions in supramolecular architectures is still a difficult task,[3] and most known dye assemblies are constructed as simple one-dimensional stacks through stacking of their π-systems to give columnar liquid crystalline phases[4] or by gelation of the solvent to give organogels.[5] In other examples, hydrogen-bonding[6] or metal−ligand coordination[7] has been applied, but in most cases neither long range ordering nor advanced

[†] Universität Würzburg.
[‡] RWTH-Aachen.

(1) Pullerits, T.; Sundström, V. *Acc. Chem. Res.* **1996**, *29*, 381−389.
(2) (a) Holzwarth, A. R.; Schaffner, K. *Photosynth. Res.* **1994**, *41*, 225−233. (b) Blankenship, R. E.; Olson, J. M.; Miller, M. In *Anoxygenic Photosynthetic Bacteria*; Blankenship, R. E., Madigan, M. T., Bauer, C. E., Eds.; Kluwer: Dordrecht, 1995; p 399. (c) Tamiaki, H. *Coord. Chem. Rev.* **1996**, *148*, 183−197. (d) Olson, J. M. *Photochem. Photobiol.* **1998**, *67*, 61−75. (e) Nozawa, T.; Ohtomo, K.; Suzuki, M.; Morishita, Y.; Madigan, M. T. *Bull. Chem. Soc. Jpn.* **1993**, *66*, 231−237.
(3) (a) Engelkamp, H.; Middelbeck, S.; Nolte, R. J. M. *Science* **1999**, *284*, 785−788. (b) De Witte, P. A. J.; Castriciano, M.; Cornelissen, J. J. L. M.; Monsù Scolaro, L.; Nolte, R. J. M.; Rowan, A. E. *Chem.—Eur. J.* **2003**, *9*, 1775−1781. (c) Haycock, R. A.; Hunter, C. A.; James, D. A.; Michelsen, U.; Sutton, L. R. *Org. Lett.* **2000**, *2*, 2435−2438. (d) Würthner, F. *Chem. Commun.* **2004**, in press.
(4) (a) Van Nostrum, C. F. *Adv. Mater.* **1996**, *8*, 1027−1030. (b) Vacus, J.; Simon, J. *Adv. Mater.* **1995**, *7*, 797−800. (c) Sautter, A.; Thalacker, C.; Würthner, F. *Angew. Chem., Int. Ed.* **2001**, *40*, 4425−4428. (d) Würthner, F.; Thalacker, C.; Diele, S.; Tschierske, C. *Chem.—Eur. J.* **2001**, *7*, 2245−2253.
(5) (a) Schoonbeek, F. S.; van Esch, J. H.; Wegewijs, B.; Rep, D. B. A.; De Haas, M. P.; Klapwijk, T. M.; Kellogg, R. M.; Feringa, B. L. *Angew. Chem., Int. Ed.* **1999**, *38*, 1393−1397. (b) Ajayaghosh, A.; George, S. J. *J. Am. Chem. Soc.* **2001**, *123*, 5148−5149. (c) Tamaru, S.; Uchino, S.; Takeuchi, M.; Ikeda, M.; Hatano, T.; Shinkai, S. *Tetrahedron Lett.* **2002**, *43*, 3751−3755. (d) Ikeda, M.; Takeuchi, M.; Shinkai, S. *Chem. Commun.* **2003**, 1354−1355. (e) Ajayagosh, A.; George, S. J.; Praveen, V. K. *Angew. Chem., Int. Ed.* **2003**, *115*, 346−349.
(6) (a) Würthner, F.; Thalacker, C.; Sautter, A. *Adv. Mater.* **1999**, *11*, 754−758. (b) Würthner, F.; Thalacker, C.; Sautter, A.; Schärtl, W.; Ibach, W.; Hollricher, O. *Chem.—Eur. J.* **2000**, *6*, 3871−3885. (c) Schenning, A. P. H. J.; Jonkheijm, P.; Peeters, E.; Meijer, E. W. *J. Am. Chem. Soc.* **2001**, *123*, 409−416. (d) Würthner, F.; Yao, S.; Heise, B.; Tschierske, C. *Chem. Commun*. **2001**, 2260−2261. (e) Yagai, S.; Karatsu, T.; Kitamura, A. *Chem. Commun*. **2003**, 1844−1845.
(7) (a) Fleischer, E. B.; Shachter, A. M. *Inorg. Chem.* **1991**, *30*, 3763−3769. (b) Milic, T. N.; Chi, N.; Yablon, D. G.; Flynn, G. W.; Batteas, J. D.; Drain, C. M. *Angew. Chem., Int. Ed.* **2002**, *41*, 2117−2119. (c) Ayabe, M.; Yamashita, K.; Sada, K.; Shinkai, S.; Ikeda, A.; Sakamoto, S.; Yamaguchi, K. *J. Org. Chem.* **2003**, *68*, 1059−1066. (d) Würthner, F.; You, C.-C.; Saha-Möller, C. R. *Chem. Soc. Rev.* **2004**, *33*, 133−146.

 10.1021/ja0496367 CCC: $27.50

functionality could be achieved. A remarkable exception is given by the since long time known *J*- (or Scheibe-) aggregates of cyanine dyes.[8] Only in water, these dyes self-assemble to mesoscopic dimensions, a behavior that is attributed to strong dispersive interactions between the π-systems and the hydrophobic effect. Owing to their unique absorption, fluorescence, and sensitization properties, various applications of these dyes became feasible in silver-halide photography, solar cells, and recently sensor devices.[9,10]

In recent years, supramolecular chemists have started to explore the formation of extended assemblies by means of directional receptor groups that are attached to the respective molecular building blocks.[11] This has led to the revival of an old concept of chemical research, i.e., the formation of supramolecular polymers.[12] Indeed, prior to Staudinger's seminal work on macromolecules, it was assumed that all highly viscous solutions and viscoelastic properties in the bulk are resulted from physical association of low molecular weight compounds. This view was corroborated by several low molecular weight organic compounds that can gel water or organic solvents at minute solute concentrations (0.1−3 wt %).[13] This effect has been used industrially to prepare greases and lubricants.[14] Gel formation depends on the presence of a network that percolates the system and confines the solvent.[15] Due to the low lateral extensions of small molecules, network formation depends generally on the self-assembly of gel forming molecules to complex superstructures. It is well-known from percolation[16] and random-contact theory[17] that the percolation threshold volume fraction can become very small for rod- or ribbon-type structures. In fact, all efficient organogelators assemble to elongated superstructures of high aspect ratio.[18] With the advancement of supramolecular chemistry, the scientific interest in such physically assembled systems has regained, and during the past 15 years, a large variety of new organogelators has been evolved[18] and numerous new applications have been proposed.[19]

Nevertheless, in contrast to high molecular weight covalent compounds ("polymers"), none of these gelator molecules is able to form a macromolecular structure already in dilute solution. Thus, it took until 1997 that the polymer-typical properties of highly viscous solutions and elastomeric behavior in an amorphous bulk state could be demonstrated for a truly supramolecular polymer based on a self-complementary quadruple hydrogen-bonding motif.[20] A very high binding constant between the monomers is of paramount importance for the realization of those macromolecule-like properties for an association polymer of small organic molecules in solution. Sijbesma, Meijer, and co-workers achieved this by an array of four hydrogen bonds per monomer−monomer contact, as well as the directionality of the binding sites which in combination with the conformational preference of the spacers favored polymerization over small cycle formation.[20] Meanwhile, more supramolecular polymers have been reported.[12] However, the combination of high binding strength, a defined and directional interaction, and synthetic simplicity is still a major challenge which limited the range of useful supramolecular interactions to other multiple hydrogen bonding motifs[21] and metal−ligand coordination[22] so far. Structurally, all given examples follow the same construction principle: The monomers contain two self-complementary receptor sites which are connected by a flexible spacer unit, the latter provides good solubility properties and supports low glass transition temperatures, e.g., the formation of an amorphous solid state. Recent investigations showed that the choice of the connector unit is of critical importance if polymer-type properties should be maintained.[12] However, introduction of functional dyes into the supramolecular polymeric chain proved to be a major challenge because the simultaneous presence of hydrogen-bonding (or metal−ligand coordination) and extended π-systems that are prone to aggregation often leads to insoluble materials with pigmentlike properties rather than those of processable polymers.[23,24]

Recently, in the course of our studies on highly dipolar merocyanine dyes (e.g., **1** and **2**) for nonlinear optical and photorefractive applications,[25] we noticed the formation of tightly bound dimer aggregates. Especially, for dyes **2** (Chart 1), a binding strength comparable to Meijer's quadruple

(8) (a) Jelley, E. *Nature* **1936**, *138*, 1009−1009. (b) Scheibe, G. *Z. Angew. Chem.* **1936**, *49*, 563−563. (c) Möbius, D. *Adv. Mater.* **1995**, *7*, 437−444. (d) Mishra, A.; Behera, R. K.; Behera, P. K.; Mishra, B. K.; Behera, G. B. *Chem. Rev.* **2000**, *100*, 1973−2011.

(9) (a) Herz, A. H. *Adv. Colloid Interface Sci.* **1977**, *8*, 237−298. (b) Kobayashi, T., Ed. *J-Aggregates*; World Scientific: Singapore, 1996.

(10) Jones, R. M.; Lu, L.; Helgeson, R.; Bergstedt, T. S.; McBranch, D. W.; Whitten, D. G. *Proc. Natl. Acad. Sci. U.S.A.* **2001**, *98*, 14769−14772.

(11) Lehn, J.-M. *Supramolecular Chemistry*; VCH: Weinheim, 1995.

(12) For recent reviews, see: (a) Brunsveld, L.; Folmer, B. J. B.; Meijer, E. W.; Sijbesma, R. P. *Chem. Rev.* **2001**, *101*, 4071−4097. (b) Ciferri, A. *Macromol. Rapid Commun.* **2002**, *23*, 511−529. (c) Schmuck, C.; Wienand, W. *Angew. Chem., Int. Ed.* **2001**, *40*, 4363−4369.

(13) (a) Lipowitz, A. *Ann. Chem. Pharm.* **1841**, *38*, 348−355. (b) Foster, M. O.; Jackson, T. *Trans. Chem. Soc.* **1907**, 1877−1890. (c) Hatschek, E. *Kolloid-Z.* **1912**, *11*, 158−165. (d) Zsigmondy, R.; Bachmann, W. *Kolloid-Z.* **1912**, *11*, 145−157. (e) Haller, R. *Kolloid-Z.* **1918**, *22*, 49−53 (f) Papkova-Kwitzel, T. P. *Kolloid-Z.* **1934**, *69*, 57−65.

(14) (a) Evans, E. A. J. *Inst. Petroleum* **1950**, *36*, 367−381. (b) Booser, E. R. *Lubrification and Lubricants − Greases in Encyclopedia of Chemical Technology*, 4th ed.; Kirk-Othmer, Ed.; Wiley-Interscience: New York, 1991; Vol. 15, pp 492−517, .

(15) (a) Ferry, J. D. *Viscoelastic Properties of Polymers*; Wiley: New York, 1980. (b) Te Nijenhuis, K. *Thermoreversible Network: viscoelastic properties and structure of gels*; Springer: Berlin, 1997.

(16) Stauffer, D.; Aharony A. *Introduction to Percolation Theory*, 2nd ed.; Taylor & Francis: London, Washington, DC, 1992.

(17) Philipse A. P. *Langmuir* **1996**, *12*, 1127−1133.

(18) (a) Terech P.; Weiss R. G. *Chem. Rev.* **1997**, *97*, 3133−3159. (b) Fuhrhop H.-J.; Köning J. *Membranes and Molecular Assemblies: the Synkinetic Approach*; Stoddart, J. F., Ed.; The Royal Society of Chemistry: Oxford, 1994.

(19) (a) Hanabusa, K.; Hiratsu, K.; Kimura, M.; Shirai, H. *Chem. Mater.* **1999**, *11*, 649−655 (b) Ono, Y.; Kanekiyo, Y.; Inoue, K.; Hojo, J.; Shinkai, S. *Chem. Lett.* **1999**, 23−24. (c) Guan, L.; Zhao, Y. *Chem. Mater.* **2000**, *12*, 3667−3673.

(20) Sijbesma, R. P.; Beijer, F. H.; Brunsveld, L.; Folmer, B. J. B.; Hirschberg, J. H. K.; Lange, R. F. M.; Lowe, J. K. L.; Meijer, E. W. *Science* **1997**, *278*, 1601−1604.

(21) (a) Castellano, R. K.; Rudkevich, D. M.; Rebek, J., Jr. *Proc. Natl. Acad. Sci. U.S.A.* **1997**, *94*, 7132−7137. (b) Castellano, R. K.; Clark, R.; Craig, S. L.; Nuckolls, C.; Rebek, J., Jr. *Proc. Natl. Acad. Sci. U.S.A.* **2000**, *97*, 12418−12421. (c) Klok, H.-A.; Jolliffe, K. A.; Schauer, C. L.; Prins, L. J.; Spatz, J. P.; Möller, M.; Timmerman, P.; Reinhoudt, D. N. *J. Am. Soc. Chem.* **1999**, *121*, 7154−7155. (d) Yamaguchi, N.; Gibson, H. W. *Angew. Chem., Int. Ed.* **1999**, *38*, 143−147. (d) Ogawa, K.; Kobuke, Y. *Angew. Chem., Int. Ed.* **2000**, *39*, 4070−4073. (e) Berl, V.; Schmutz, M.; Krische, M. J.; Khoury, R. G.; Lehn, J.-M. *Chem.−Eur. J.* **2002**, *8*, 1227−1244.

(22) (a) Rehahn, M. *Acta Polymer* **1998**, *49*, 201−224. (b) Michelsen, U.; Hunter, C. A. *Angew. Chem., Int. Ed.* **2000**, *39*, 764−767. (c) Dobrawa, R.; Würthner, F. *Chem. Commun.* **2002**, 1878−1879. For a number of coordination polymers it is not yet clear if their formation takes place in a reversible manner which is considered as the signature of a "supramolecular" polymer in contrast to strong and irreversible linkages of ordinary polymers.

(23) The combination of at least two rather strong intermolecular interactions such as $\pi-\pi$ aggregation and hydrogen bonding (or metal−ligand coordination) is exactly the approach used by chemists designing insoluble organic pigments. See: Herbst, W.; Hunger, K. *Industrial Organic Pigments*, 2nd ed.; VCH: Weinheim, 1997.

(24) For recent successful work, see: Sijbesma, R. P.; Meijer, E. W. *Chem. Commun.* **2003**, 5−16.

(25) (a) Würthner, F.; Wortmann, R.; Meerholz, K. *Chem. Phys. Chem.* **2002**, *3*, 17−31. (b) Würthner, F.; Yao, S.; Schilling, J.; Wortmann, R.; Redi-Abshiro, M.; Mecher, E.; Gallego-Gomez, F.; Meerholz, K. *J. Am. Chem. Soc.* **2001**, *123*, 2810−2814.

Chart 1

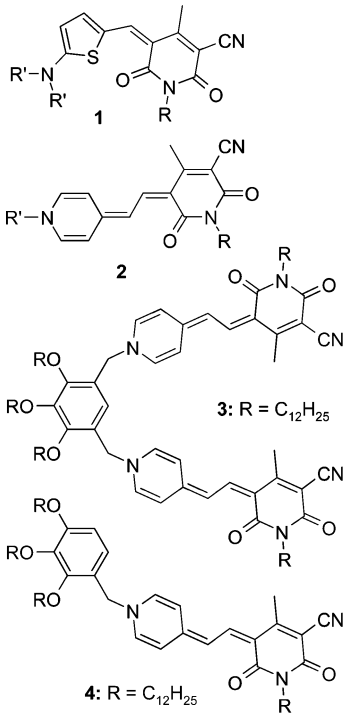

hydrogen bonds in low polarity solvents was observed.[26] Thus, dimerization constants of 1.4×10^6 M^{-1} in dioxane and 2.1×10^7 M^{-1} in tetrachloromethane were measured at 25 °C, and a value of about 10^8 M^{-1} may be estimated for aliphatic solvents from the permittivity dependence of the dimerization constant.[27] In addition, we could confirm that the structure of these dimer aggregates are highly defined and exhibit little dependence on substituents making these dipolar interactions directional and, therefore, highly promising candidates for supramolecular polymers bearing functional π-systems. Based on this work and molecular modeling, we designed dye **3** whose capability for noncovalent polymerization was recently communicated[28] and will be discussed in detail here.

Results

Synthesis. Bis(merocyanine) dye **3** was prepared according to Scheme 1. The synthesis started with 2-fold bromomethylation of 1,2,3-tris(*n*-dodecyloxy)benzene **5** to yield intermediate **6**, using a general bromomethylation procedure for aromatic compounds.[29] Heating of **6** with 4-methylpyridine in acetonitrile at reflux readily afforded dipyridinium salt **7**. Dye **3** was obtained by subsequent reaction of pyridone **9** with *N*,*N*′-diphenylformamidine and **7**, a method that has been applied for the synthesis of other merocyanine dyes in our earlier work.[30] Monofunctional dye **4** was synthesized as a reference compound using a similar procedure (Scheme 1).

Scheme 1. Synthesis of the Dyes **3** and **4**

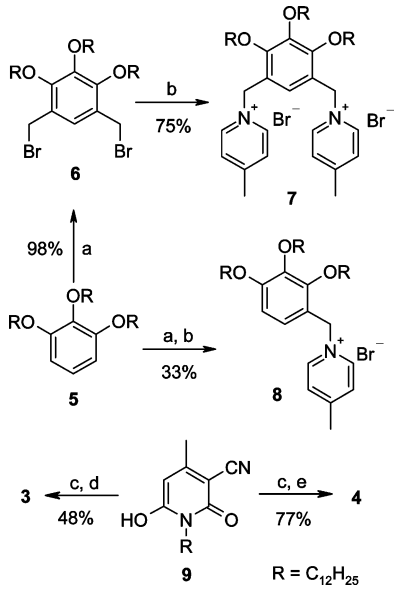

(a) Paraformaldehyde, HOAc, HBr, 70 °C, 120 h. (b) 4-Methylpyridine, CH_3CN, reflux, 24 h. (c) *N*,*N*′-Diphenylformamidine, Ac_2O, room temperature to 90 °C, 30 min. (d) **7**, KOAc, 100 °C, 20 h. (e) **8**, KOAc, 100 °C, 20 h.

UV/vis Aggregation Studies. UV/vis spectroscopy has been extensively utilized to study dye aggregation in solution. With this method, electronic interactions between the π−conjugated systems of the dyes are elucidated and the concentration range for aggregate formation is easily assessed. For simple processes such as dimerization or the formation of an extended columnar aggregate, binding constants and Gibbs binding energies may be obtained from these data.[31] In addition, structural information is accessible from the splitting of the absorption band due to the excitonic coupling.[32] However, only in simple cases the information gained from the absorption changes suffices to derive a reliable model of aggregate size and geometry. For this reason, conclusive structural models have sparsely been proposed, even for the extensively studied dye aggregates that have been known for a long time.

In our earlier work, we have studied the aggregation behavior of merocyanine dyes **1** and **2** by several methods employing a significant number of solvents and found that in this case a quite simple situation is given. Owing to the high dipolarity of these dyes, electrostatic interactions are the dominant driving force for aggregation. They lead to the formation of centrosymmetric dimers with antiparallel dipole moments as established for all solvents investigated and in the solid state as well. From the concentration range at which aggregation takes place, we could calculate the dimerization constants and show that these are highest in less polar solvents, i.e., $K > 10^7$ M^{-1} in tetrachloromethane and smallest in polar solvents, i.e., $K = 65$ M^{-1} in THF.

Accordingly, aggregation of dyes **2** takes place already in the micromolar regime in tetrachloromethane but only in the millimolar regime in THF. The same behavior is observed for dye **4** demonstrating that the tris(*n*-dodecyloxy)benzyl group

(26) (a) Würthner, F.; Yao, S. *Angew. Chem., Int. Ed.* **2000**, *39*, 1978−1981. (b) Würthner, F.; Yao, S.; Debaerdemaeker, T.; Wortmann, R. *J. Am. Chem. Soc.* **2002**, *124*, 9431−9447.
(27) The exact values for the calculated dimerization constants are 2.1×10^8 M^{-1} in *n*-hexane ($\epsilon_r = 1.88$) and 6×10^7 M^{-1} in cyclohexane ($\epsilon_r = 2.02$) at 298 K.
(28) Würthner, F.; Yao, S.; Beginn, U. *Angew. Chem., Int. Ed.* **2003**, *42*, 3247−3250.
(29) (a) van der Made, A. W.; van der Made, R. H. *J. Org. Chem.* **1993**, *58*, 1262. (b) Wang, B.; Wasielewski, M. R. *J. Am. Chem. Soc.* **1997**, *119*, 12−21.
(30) Würthner, F. *Synthesis* **1999**, 2103−2113.
(31) (a) Connors, K. A. *Binding Constants*; Wiley: New York, 1987. (b) Martin, R. B. *Chem. Rev.* **1996**, *96*, 3043−3064.
(32) (a) McRae, E. G.; Kasha, M. *Physical Process in Radiation Biology*; Acadamic Press: New York, 1964; pp 17−42. (b) Kasha, M.; Rawls, H. R.; El-Bayoumi, M. A. *Pure Appl. Chem.* **1965**, *11*, 371−392.

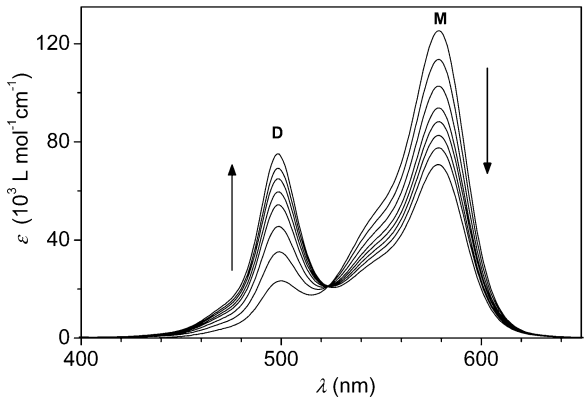

Figure 1. Concentration-dependent UV/vis absorption spectra of dye **4** in trichloroethene. The arrows indicate changes upon increasing concentration from 1.3×10^{-6} M to 4.3×10^{-5} M.

has little influence on the dimerization equilibrium. Figure 1 shows the aggregation of dye **4** in trichloroethene (TCE) ($\epsilon_r =$ 3.39), a solvent whose polarity lies between that of methylcyclohexane ($\epsilon_r = 2.02$) and dichloromethane ($\epsilon_r = 8.93$, all values at 25 °C). In dilute solutions, the most prominent band appears at 579 nm that can be undoubtedly assigned to the monomeric dyes (M-band). At higher concentration, dimerization takes place as indicated by a new hypsochromically shifted band at 497 nm (D-band). A well-defined isosbestic point at 523 nm confirms the presence of a two-state equilibrium and allows the determination of a dimerization constant of $K =$ 30 000 M^{-1}. For the same concentration range in the more polar solvent dichloromethane, only the monomeric species is present ($\lambda_{max} = 550$ nm, $\epsilon_{max} = 117\,000$ L $mol^{-1}cm^{-1}$), whereas, in the less polar solvent methylcyclohexane, only the dimer band is observed ($\lambda_{max} = 483$ nm, $\epsilon_{max} = 100\,000$ L $mol^{-1}cm^{-1}$).

For the bis(merocyanine) dye **3**, the situation becomes more complicated because the two π-systems could aggregate *intra*molecularly ("folding") or *inter*molecularly leading to cyclic or linear oligomers and polymers. Intramolecular folding of tethered merocyanine dyes has recently been studied by Whitten and co-workers and Okazaki and co-workers.[33] However, for the topology given in bis(merocyanine) **3**, such folding seems unlikely because intramolecular aggregation would result in parallel stacking of the two dipolar dyes that is considered to be energetically a very disfavored process (Scheme 2). Experimental support for this conclusion is given from the UV/vis absorption spectra in dichloromethane at concentrations $< 10^{-5}$ M where only nonaggregated π-systems are observed (Figure 2).

Under these conditions, bis(merocyanine) **3** exhibits about twice the absorbance as merocyanine **4**, and no evidence for a close intramolecular contact of the π-systems is given. Upon closer inspection we notice that the absorption maximum of dye **4** compared to dye **3** is red-shifted by 16 nm. Such a red shift (that is also found in THF) is in accordance with a weak *J*-type intramolecular coupling that arises if the two merocyanine dyes are in a conformation where their dipole moments point to the opposite direction as expected from the electrostatic considerations above (Scheme 2). On the basis of Whitten's and Okazaki's work,[33] this conformation should be even more favored in less polar solvents owing to smaller solvation energies for the dipolar subunits. Accordingly, for such solvents bis(merocyanine) **3** is considered to exist in a rigid and highly preorganized conformation suitable for intermolecular aggregation as proposed in Scheme 2.

For bis(merocyanine) dyes **3**, this aggregation can already be observed in dichloromethane where a D-band appears at 491 nm at concentrations between 10^{-5} and 10^{-4} M. An isosbestic point at 526 nm indicates a two-state equilibrium (see Supporting Information). Notably for dye **4** no changes in the UV/vis spectrum is observed up to a concentration of 10^{-3} M in this solvent.[34] However, dissolution of dye **3** in less polar solvents revealed a rather new situation that was unprecedented for the monomeric dyes **1**[26] and **4**. Figure 2 compares UV/vis absorption spectra of dye **3** at an identical concentration of 10^{-5} M in different solvents. Within the series of solvents of intermediate polarity dichloromethane ($\epsilon_r = 8.93$), THF ($\epsilon_r = 7.52$), chloroform ($\epsilon_r = 4.81$), and TCE ($\epsilon_r = 3.39$), a gradual transition from monomeric to D-aggregated species can be seen pointing at an oligomerization process that would ultimately lead to a polymer when all merocyanine dyes are paired within a dimeric unit (Scheme 2). However, for the least polar solvents, tetrachloromethane ($\epsilon_r = 2.24$) and methylcyclohexane ($\epsilon_r = 2.02$) where such a situation was expected, a completely new band appeared at 442 nm (MCH) or 446 nm (CCl_4) that is signified by a much more pronounced hypsochromic shift compared to the absorption of the monomeric dye and a very narrow bandwidth. Both observations are highly indicative for the existence of a higher order aggregate where the dyes exhibit excitonic coupling to more than one closest neighbor dye. In accordance with the literature, this narrow and intense band is called as an H-band[9,35] that arises from additional excitonic coupling to other dye molecules that are organized in close proximity to the dimeric unit. Next, we investigated the emergence of this H-aggregated species by addition of MCH to solutions of **3** in THF and vice versa at a constant concentration of 10^{-5} M. This procedure seemed to be promising because these solvents are miscible at any composition and one (MCH) contains the pure H-aggregated species whereas the other (THF) contains the nonaggregated dye in equilibrium with small amounts of the D-aggregate.

As can be seen from Figure 3 upon increasing the amount of MCH, two transitions take place. The first transition occurs between 0% MCH and 39% MCH (red lines) with a quasi-isosbestic point at 511 nm. From here a slight increase of the MCH content leads to the abrupt formation of the H-aggregate (again signified by a quasi-isosbestic point at 464 nm, black lines) that is already the dominating species at 46% MCH (cf. Figure 3b). Remarkably, these conversions among M-, D-, and H-species are fully reversible within less than a few minutes at

(33) (a) Lu, L.; Lachicotte, R. J.; Penner, T. L.; Perlstein, J.; Whitten, D. G. *J. Am. Chem. Soc.* **1999**, *121*, 8146−8156. (b) Katoh, T.; Inagaki, Y.; Okazaki, R. *J. Am. Chem. Soc.* **1998**, *120*, 3623−3628.

(34) If the changes in the absorbance of bis(merocyanine) dye **3** in dichloromethane are treated in a dimerization model, a binding constant of 1.5×10^4 M^{-1} is obtained. Because this value is 2 orders of magnitude larger than the value of the monomeric merocyanine dyes (cf. ref 26) in this highly polar solvent, it might indicate the formation of cyclic oligomers. Formation of such oligomers is favored at low concentration if the effective molarity is favorable; see: Ercolani, G. *J. Phys. Chem. B* **1998**, *102*, 5699. Further studies in the low concentration range of **3** and related bis(merocyanine) dyes are in progress and will be reported elsewhere.

(35) (a) Herz. A. H. *Photogr. Sci. Eng.* **1974**, *18*, 323−325. (b) West, W.; Lovel, S.; Cooper, W. *Photogr. Sci. Eng.* **1970**, *14*, 52. (c) West, W.; Lovel, S.; Cooper, W. *Photogr. Sci. Eng.* **1970**, *14*, 184. (d) Emerson, E.; Conlin, M.; Rosenoff, A.; Norland, K.; Rodriguez, H.; Chin, D.; Bird, G. J. *Phys. Chem.* **1967**, *71*, 2396.

Scheme 2. Model for the Formation of Dimer Aggregates of Merocyanine Dye **4** and the Related Supramolecular Polymerization Process of Bis(merocyanine) Dyes **3** by Means of Dipolar Aggregation

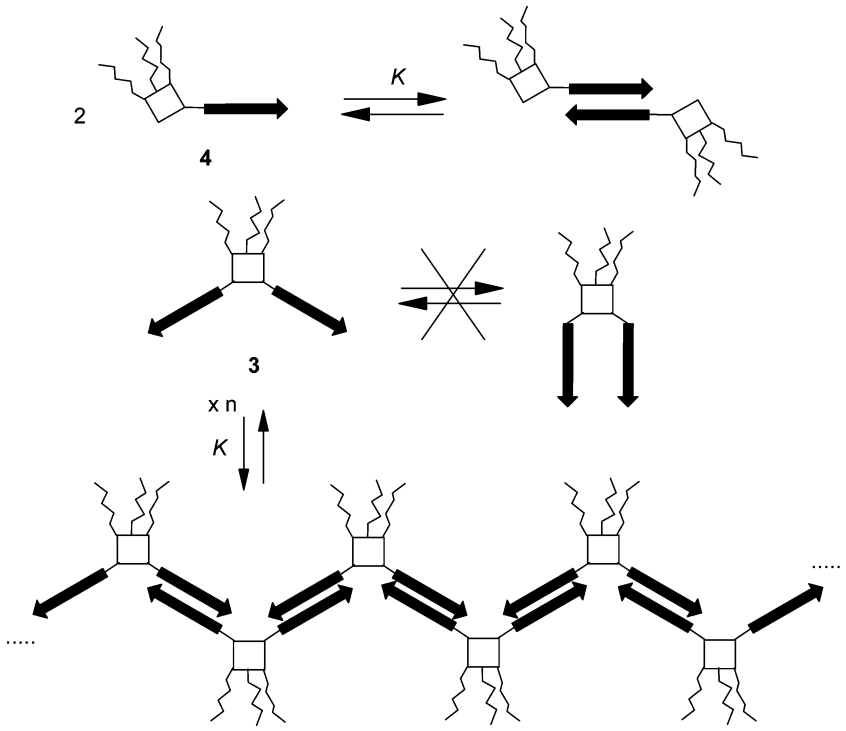

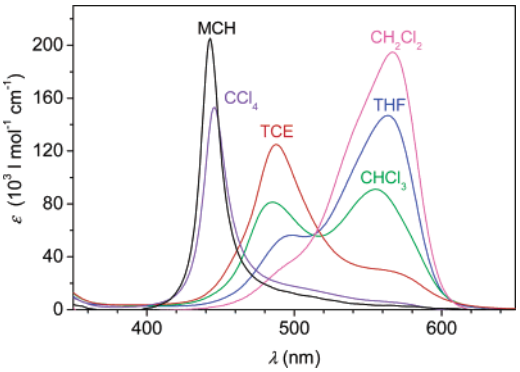

Figure 2. UV/vis absorption spectra of 10^{-5} M solutions of dye **3** at 293 K in pure solvents of different polarity.

room temperature as the same spectra are obtained starting from 10^{-4} M stock solutions of **3** in pure MCH or in pure THF by addition of the other solvent.

This reversibility could also be confirmed by temperature-dependent studies for a MCH/THF = 42:58 (wt %) mixture as depicted in Figure 4. At this composition we see the transition from the H- to the D-aggregate in the temperature range between 2 and 50 °C with a "melting point" of about 25 °C. However, at lower temperatures (<20 °C), full equilibration required a longer time in the range from several minutes (20 °C) up to hours (2 °C). Another noteworthy observation was made for solutions of **3** in pure MCH. In this solvent H-aggregates are the only species at any concentration > 10^{-7} M, but at higher concentration the H-band became more narrow and shifted to a slightly shorter wavelength, i.e., from 445 nm (ϵ_{max} = 177 000 L mol^{-1} cm^{-1}) at 5 × 10^{-6} M to 442 nm (ϵ_{max} = 205 000 L mol^{-1} cm^{-1}) at 2 × 10^{-5} M (Supporting Information).

All these observations are indicative for the formation of more tightly packed dyes within a higher order superstructure in a hierarchical process upon decreasing the solvent polarity and increasing the dye concentration. However, solely based on UV/vis absorption data, no structural information of these higher order aggregates can be deduced.

Kinetic Studies. The aggregation process observed for THF/MCH mixtures upon changing the solvent composition was shown to be fully reversible. Low activation energies are indeed expected based on binding constants in the range of 10^8 M^{-1} if the supramolecular polymer is composed of independent chromophore pairing processes as proposed in Scheme 2. On the other hand, formation of higher order aggregates by means of additional noncovalent interactions between individual polymeric strands should be associated with a considerably higher activation barrier.

The long equilibration time at lower temperatures in MCH/THF mixtures was a clear indication for an enhanced kinetic stability of the H-aggregated state. Even more remarkable was the behavior observed if dye **3** was dissolved in pure TCE. Here a freshly prepared solution exhibited the signature of the H-aggregated state which, however, transformed into the D-aggregate within a time period between hours and days depending on the temperature (Figure 5A).

Figure 5B shows the kinetic analysis of the transition of the H-aggregated into the D-aggregated species applying a first-order reaction model giving rate constants between 8.3 × 10^{-4} min^{-1} (12 °C) and 2 × 10^{-2} min^{-1} (42 °C). From the slope and the Arrhenius eq 1,

$$\ln(k_{diss}) = -\frac{E_a}{RT} + C \qquad (1)$$

where k_{diss} denotes the reaction rate constant, E_a is the activation energy, T is the temperature, R is the molar gas constant, and C is a constant; an activation energy of 77 kJ/mol is calculated for the transformation of the H- into the D-aggregate.

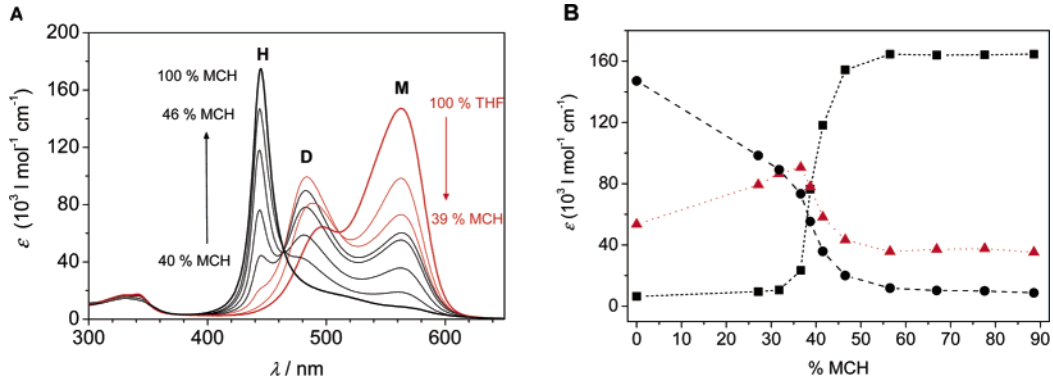

Figure 3. (A) UV/vis absorption spectra of 10^{-5} M solutions of dye **3** in MCH/THF mixtures at 293 K. (B) Absorbance at three characteristic wavelengths in different solvent compositions showing the abrupt transition to H-aggregates at ~40 wt % MCH: 444 nm (■), 484 nm (▲), 563 nm (●).

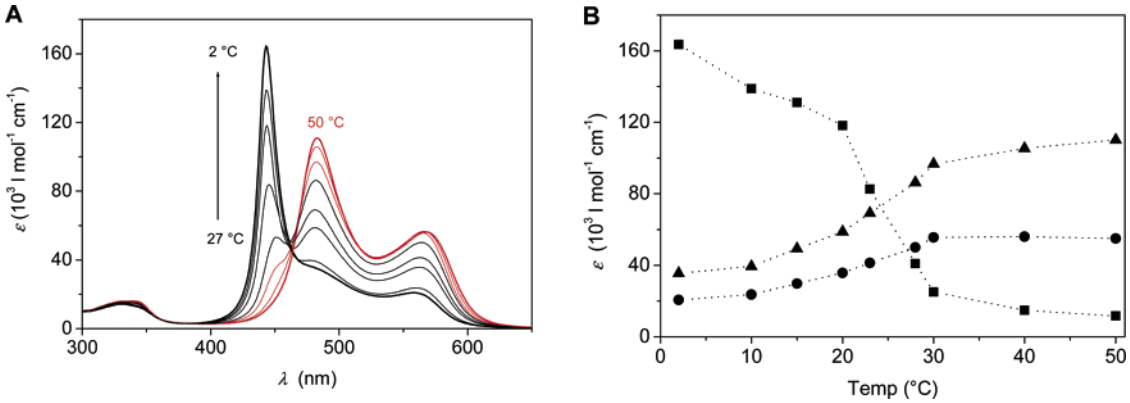

Figure 4. (A) Temperature-dependent UV/vis absorption spectra at 10^{-5} M concentration of dye **3** in a mixture of MCH/THF = 42:58 (wt %) and (B) absorbance at three characteristic wavelengths: 444 nm (■), 481 nm (▲), 562 nm (●).

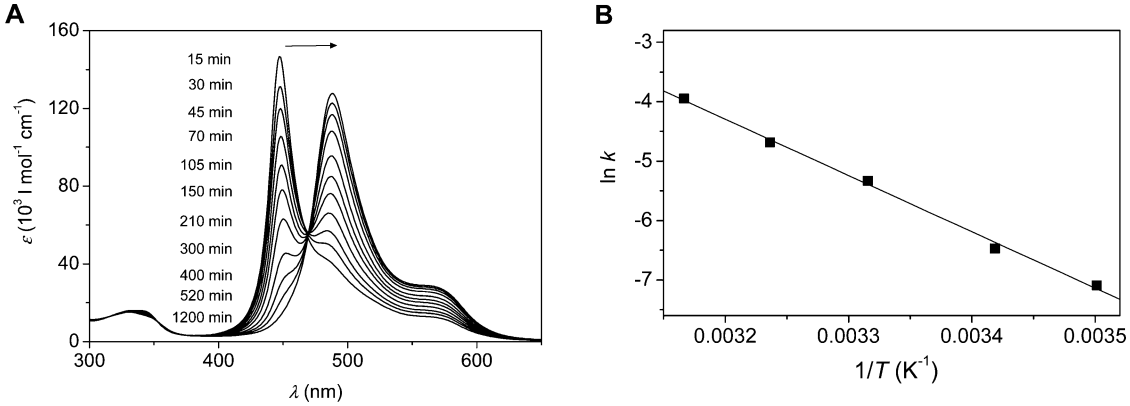

Figure 5. (A) Time-dependent transition from the H-aggregated species into the D-aggregated species for dye **3** at 10^{-5} M in trichloroethene at 30 °C. (B) Van't Hoff plot of $\ln(k_{diss})$ versus $1/T$ for the disassembly of H-aggregates of dye **3** in trichloroethene.

These experiments clearly revealed that the H-aggregated state is not the thermodynamically most stable one in chlorinated solvents which are able to solvate π-conjugated systems by means of strong dispersion interactions and that the kinetic barrier for disassembly is pretty high in solvents of low permittivity where dipolar forces between antiparallel dye pairs are large. In accordance with this notion, no disassembly of the H-aggregate could be observed in the least polar chlorinated solvent tetrachloromethane (Supporting Information).

Viscosity Measurements. The viscosities of 0.5 to 3.3 mM MCH solutions ($c < 5$ g L^{-1}) of compounds **3**, **4**, and mixtures thereof have been measured at 30 °C by means of a capillary viscosimeter. Huggin's plots of the reduced viscosities η_{red} versus the concentration are depicted in Figure 6. As a reference experiment, the reduced viscosity of the monofunctional dye **4** was examined first. From UV/vis experiments discussed before, it is evident that only dimers $(\mathbf{4})_2$ could be formed in the respective concentration regime. In fact, the reduced viscosities were smaller than 1.5 mL g^{-1}, almost without any concentration dependence of η_{red}. This behavior clearly indicated the presence of only low molecular weight species (Figure 6, curve d). However, the bifunctional dye **3** formed highly viscous solutions in MCH: With dye **3** the values of η_{red} exceeded 0.65 L g^{-1}, which is typical for macromolecular solutions (e.g., poly(butadiene), $M_n = 10^6$ g/mol; $[\eta]_{cyclohexane}$, 20 °C = 0.57 L g^{-1}).[36] The curve exhibited two clearly distinguished slopes. Below a dye content of 3 g L^{-1}, a slope of 0.01 was found, while, at higher concentrations, the slope abruptly increased by

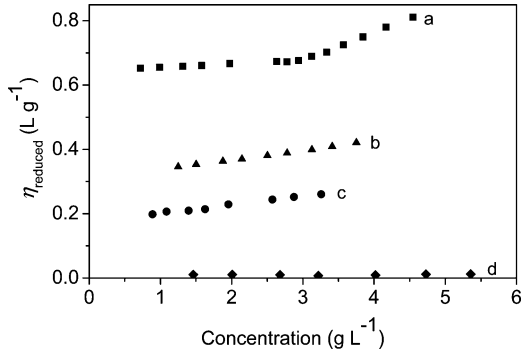

Figure 6. Reduced viscosities of solutions of dyes **3** and **4** versus concentration (grams per liter) in methylcyclohexane at 30 °C. Pure dye **3** (■); dye **3** + 10 mol % dye **4** (▲); dye **3** + 20 mol % dye **4** (●); pure dye **4** (◆).

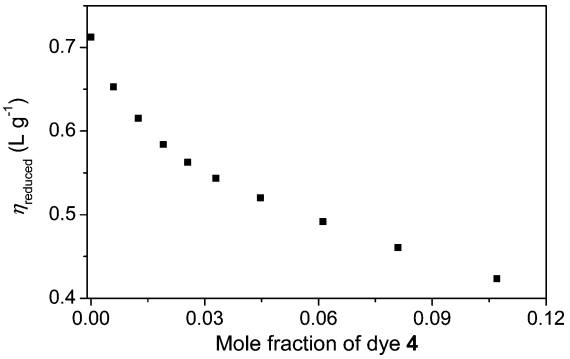

Figure 7. Effect of added dye **4** on the reduced viscosity of a 2.5×10^{-3} mol L^{-1} solution of dye **3** in methylcyclohexane.

a factor of 9 within a narrow concentration regime (cf. Figure 6, curve a).

Since the concentration series were obtained by dilution of the more concentrated solutions in the viscosimeter, the relative constancy of the reduced viscosity at low concentrations indicated that the molecular weight of the aggregates was hardly affected by lowering the dye concentration. Consequently, the thermodynamic stability of the aggregates must be very high. Although these supramolecular polymers are based on physical interactions, they may not be termed as "living" or "reversible" in the sense that they immediately react on alterations of their environment (e.g., changes in concentration or temperature).

Further measurements revealed the effect of adding monofunctional dye **4** to solutions of **3**. Coordination of such monofunctional dyes at a binding site of the bismerocyanine dye is considered to terminate the polymeric chain. According to Figure 6, as little as 10 mol % **4** reduced η_{red} roughly by a factor of 2 (Figure 6, curve b), while 20 mol % of **4** limited η_{red} to 0.25 L g^{-1} (Figure 6, curve c). In both cases, a linear concentration dependency with a uniform slope of 0.03 was observed.

Figure 7 shows how an increasing molar fraction of **4** in solutions of **3** reduced η_{red} at a constant overall dye concentration of 0.025 M. A steep drop in viscosity was observed upon addition of small amounts of dye **4**. On exceeding 4 mol % of **4** in solutions of **3**, η_{red} declined linearly with the increasing molar fraction of **4** ($d\eta_{red}/dx_4 = -1.550$ L g^{-1}). The viscosity data suggest that **3** undergoes a physical (i.e., noncovalent) polymerization in MCH, as confirmed by addition of **4**: The monofunctional dye **4** acts as a chain terminator, and it is well-known from the statistics of step polymerizations that minor amounts of monofunctional monomers will strongly diminish the maximal degree of polymerization.

The reduced viscosities were also measured for freshly prepared TCE solutions of dye **3** where the H-aggregated state was still dominating according to UV/Vis spectroscopy. Nevertheless, in this solvent, η_{red} was less than 30 mL g^{-1}, at concentrations lower than 4.0 g L^{-1}. Thus, despite the fact that an H-band was detected in the UV/vis spectrum in this concentration range, the size of the aggregated species was not large enough to provide the viscosity behavior of a polymer. The reduction of η_{red} by a factor of 20 by merely altering the solvent is an additional indication for the physical nature of these polymers. The observed lower viscosities in TCE are in accordance with our kinetic studies confirming that the H-aggregates are not thermodynamically stable in this solvent. Accordingly, when shearing forces are playing a role in the viscosimeter, disruption of the dye aggregates may take place. But also from the thermodynamic point of view, dipolar dye aggregates in TCE are significantly weaker than in MCH. From our earlier study on the solvent effect on the dimerization constant of dyes **2**, we could derive a relationship between the Gibbs energy of dimerization ΔG_{dim} and the permittivity of the solvent ϵ_r which suggests that ΔG_{dim}(MCH) $\approx 2 \times \Delta G_{dim}$ (TCE) and K_{dim}(MCH) $\approx 3000 \times K_{dim}$(TCE). Thus, the assembly in MCH is considered to be much more stable and larger in size at a given concentration.

On exceeding concentrations of 1.2 wt % (corresponds to 9 g L^{-1} or 6 mM), dye **3** formed thermoreversible gels in MCH and cyclohexane below −18 °C. In *n*-alkanes, such as *n*-hexane, *n*-octane, and *n*-dodecane, thixotropic organogels were also identified at concentrations beyond 1 wt % at room temperature. The UV/vis spectra of all alkane gels were characterized by a strong H-band similar to those observed for dilute MCH solution. At such high concentrations, obviously extended networks have developed that confine solvent molecules.

The two rheologic criteria required for a gel are (i) the independence of the dynamic elastic modulus, G', on the oscillatory frequency and (ii) G' exceeding the loss modulus G'' by about 1 order of magnitude.[15,37] The dynamic mechanical data of a **3**/*n*-octane gel, obtained from a stress controlled rheometer (experimental part), are depicted in Figure 8 revealing the typical linear viscoelastic behavior of a weak gel.[15,18]

Both the dynamic moduli, G' and G'', displayed only a weak linear increase with frequency (slopes: $n \approx 0.09$), whereas the complex viscosity, η^*, followed a straight line with a slope of −0.92. These values agree to the theory of linear viscoelasticity, predicting the sum of the absolute values of both the slopes to equal one.[37] Over the whole range of measured frequency G' exceeded G'' by a factor of 7−8.

It has to be emphasized that these gels were very fragile and the linear viscoelastic behavior could only be measured at very low shear stress values. In Figure 9 are shown the dependencies of the dynamic moduli of the dye **3**/*n*-octane gel on the applied shear stress. Only up to ca. 2 Pa the modulus of the gel was independent of the applied stress. At higher stress values, a sharp

(36) Lechner, D.; Gehrke, K.; Nordmeier, E. H. *Makromolekulare Chemie*, 2nd ed.; Birkhäuser Verlag: Basel, 1993, p 264.

(37) Kavanagh, G. M.; Ross-Murphy, S. B. *Prog. Polym. Sci.* **1998**, *23*, 533−562.

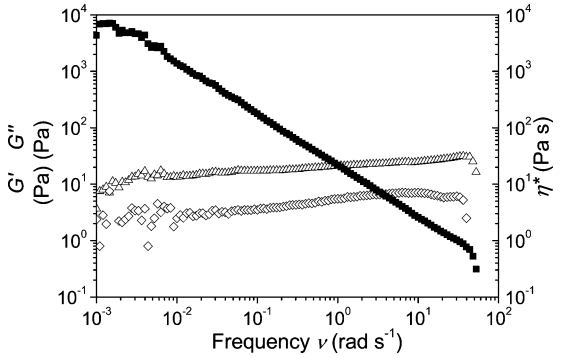

Figure 8. Dynamic moduli, $G'(\triangle)$ and $G''(\diamond)$, and complex viscosity, $\eta^*(\blacksquare)$, vs angular frequency on double logarithmic scale for a 1.2 wt % (8×10^{-3} mol L^{-1}) gel of dye **3** in *n*-octane at 25 °C. Stress amplitude $\sigma_0 = 0.1$ Pa.

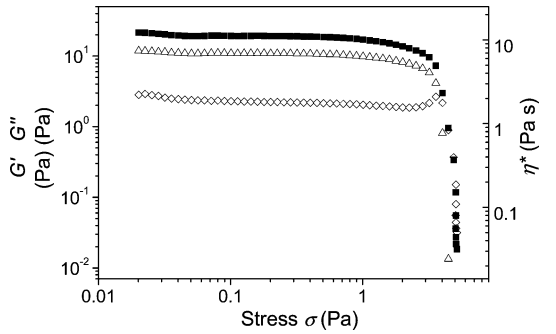

Figure 9. Dynamic module, $G'(\triangle)$ and $G''(\diamond)$, and complex viscosity, $\eta^*(\blacksquare)$, vs stress amplitude on double logarithmic scale for a 1.2 wt % (8×10^{-3} mol L^{-1}) gel of dye **3** in *n*-octane at 25 °C. Frequency $\nu = 1$ rad/s.

decrease of G' and η^* was observed. In the linear regime, the elastic structure is assumed to show a continuous recovery toward the original equilibrium structure. At higher levels of strain, the 3D structure was disrupted and major changes in the orientation and connectivity among the domains occurred and, thus, sharply reduced the elastic modulus. Note that at high stresses the storage modulus G' falls much faster than the loss modulus G'', indicating the 3D cohesion to alter into a more liquidlike system. Some recovery of gel structure took place slowly after the shear stress was released. Subsequently, to the destruction of the gel structure by application of a large stress ($\sigma = 2$ Pa), the value of G' was followed at a frequency of 0.1 Hz over a period of 1 h. During this time, about 40% of the original value of G' was regained.

The morphology of the gel was investigated by cryogenic temperature transmission electron microscopy (cryo-TEM). This technique can avoid crystallization of the solvent or rearrangement of the assemblies by ultrafast cooling. The electron micrograph of gels of dye **3** in *n*-hexane (Figure 10) displays a dense three-dimensional pattern composed of randomly oriented and intertwined fibrous bundles. At irregular intervals the bundles fuse and split to form junction zones, which stabilize the three-dimensional entangled network structures. The thicker bundles are built up from thinner rods (Figure 10, inset), the smallest resolved entities having diameters of about 10−15 nm (see arrow) which include, however, a few nanometers from the platinum shadowing. Though it is not possible to trace the fiber from beginning to end, an average length of about 2 μm could be reliably estimated and the rodlike morphology of the *H*-aggregates is clearly confirmed.

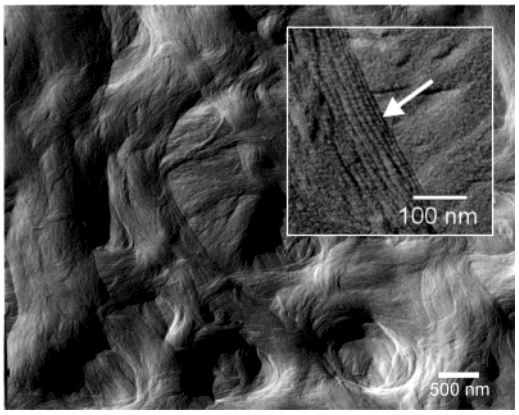

Figure 10. Cryo-TEM picture (negative) of a gel of dye **3** in *n*-hexane at a concentration of 6.5×10^{-3} M (0.97 wt %). The inset shows a magnification resolving elementary fibers of the gel.

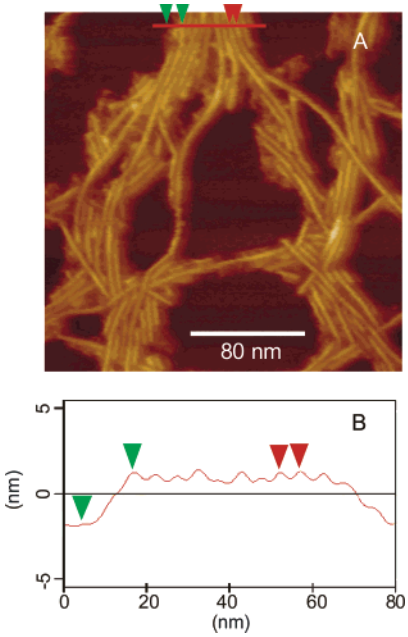

Figure 11. (A) AFM image of a sample of bis(merocyanine) dye **3** (10^{-4} M in MCH) spin-coated onto HOPG (*z* range is 30 nm). The cross section analysis of the red line in part A is presented in part B: the green and red markers show the way of the evaluation of the rods' heights and widths, respectively.

The aggregates of bis(merocyanine) dye **3** were further investigated by atomic force microscopy (AFM). For this purpose, MCH solutions of **3** were spin-coated onto a highly ordered pyrolytic graphite (HOPG) and studied by AFM operating in tapping mode. High resolution AFM images clearly show the formation of uniform structures under these experimental conditions. A typical AFM image is shown in Figure 11 A. The appearance of rather straight rods confirms the high rigidity of these assemblies. Direct sizing of the heights of the rods (Figure 11 B) from the AFM images revealed a mean value of 3.4 ± 0.1 nm. AFM investigations demonstrate that the individual rod elements tend to contact with each other to form bundles. In those cases, where the rods in bundles lie close to each other, we have also measured the lateral distances (red markers in Figure 11 B). Analysis of the distances between neighboring rods revealed a mean value of 4.8 ± 0.1 nm. The difference between the measured height and width of the rods

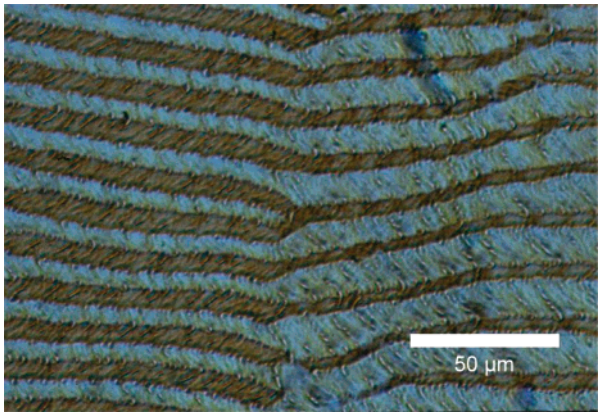

Figure 12. Optical textures of a film cast from a solution of dye **3** in methylcyclohexane.

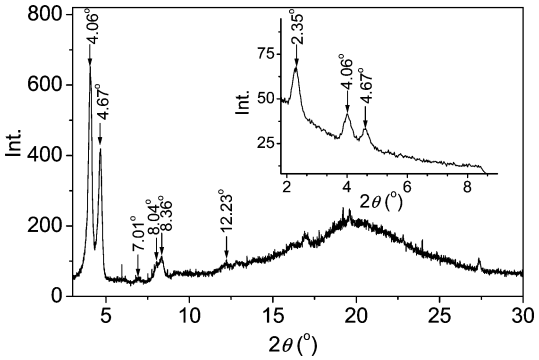

Figure 13. Wide angle X-ray scattering (WAXS) diagram of a film cast from MCH solution of dye **3** on aluminum foil. The peaks at 16.90° and 27.35° origin from the aluminum substrate, confirmed by a blank experiment. Inset: Small angle X-ray scattering (SAXS) diagram of the same film.

can be explained in terms of the indentation of the AFM tip that leads to the reduction of the apparent heights.

In MCH, at high concentration, a viscous fluid birefringent phase was observed under the optical microscope at crossed polarizers, which suggests the formation of a lyotropic mesophase. Upon further evaporation, the obtained film displays regular strip textures as shown in Figure 12. UV/vis spectra of this film exhibit the usual H-aggregate band at λ_{max}= 456 nm with a broad tailing at longer wavelength up to 650 nm (Supporting Information).

In this texture, the interval distance is between 2 and 7 μm, the scale at the same order of the length of the fibers in TEM. The molecular order of translucent films made by slow evaporation of MCH solutions of dye **3** was finally determined by X-ray scattering. Figure 13 depicts the wide and small angle X-ray scattering (WAXS and SAXS) diagram of such a film. The observed peaks are fully consistent with the calculated data according to a hexagonal columnar arrangement of rods at a distance of 4.34 nm (Table 1). The diffuse halo in the wide-angle region corresponds to the liquidlike behavior of the surrounding alkyl chains. Films prepared from *n*-octane solution afforded the same diffraction pattern. It is noteworthy that these birefringent patterns are very stable. In fact, they persist until the melting point (288 °C). Above this temperature, the compound decomposes which obstructed characterization of the isotropization transition by differential scanning calorimetry (DSC).

Table 1. Experimental and Calculated X-ray Diffraction Angles for a Columnar Hexagonal Mesophase of Bis(merocyanine) Dye **3** Exhibiting an Intercolumnar Distance of 4.34 nm

	$2\theta_{calc}$/deg	$2\theta_{exp}$/deg
(100)	2.35	2.35
(110)	4.07	4.06
(200)	4.70	4.67
(220)	8.14	8.04
(300)	7.05	6.92
(310)	8.48	8.36
(330)	12.23	12.23

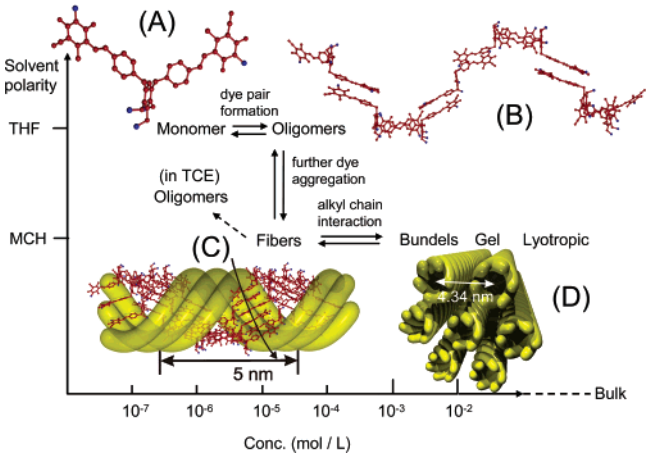

Figure 14. Structural models for the different levels of organization observed for bis(merocyanine) dye **3** in dependence on the solvent polarity and the concentration. In MCH/THF mixtures, all processes can be controlled in a reversible manner at ambient temperature. (A) Monomer according to MM+ force field calculations. For clarity, in the drawing, all dodecyl substituents are replaced by methyl groups (marked in blue) and hydrogens are omitted. (B) Polymeric chain constituted by antiparallel pairing of merocyanine dyes, calculated by MM+. (C) Tubular fiber consisting of H-aggregated dyes. The arrow around the fiber indicates the direction of H-aggregation with a closer and a more distant antiparallel dye neighbor. Note that the dodecyl chains attached to the xylylene spacer (blue) point outward and that for simplicity only one of the two possible helical aggregates (which are apparently formed in equal amounts) is shown. (D) Hexagonal packing of the rods at a distance of 4.34 nm (in this case also only one helical conformation has been chosen tentatively).

Discussion

Our studies have revealed a hierarchical self-assembly process that takes place for the π-conjugated supramolecular building block **3** upon increasing concentration and reduction of the solvent polarity. Especially the latter offered a unique parameter to control dye self-organization based on thermodynamic data derived from our earlier studies on merocyanine dimerization[28] that established the predominantly electrostatic nature of the noncovalent interaction between dipolar merocyanine dyes. Thus, with decreasing solvent polarity, the binding strength of the noncovalent "dipole−dipole" bonding increases, allowing for structural growth from the molecular to the macroscopic scale. In the present work, the formation of these structures was investigated by various techniques that allowed us to establish a fully consistent picture for the different processes of superstructure formation from dilute solution to the bulk phase (Figure 14). These processes will now be discussed starting from the monomeric compounds moving up the ladder of hierarchy.

In polar solvents bis(merocyanine) dyes **3** are dissolved as monomeric compounds (Figure 14A). This situation is given for THF up to a concentration of about 10^{-6} M and for DCM

up to a concentration of 10^{-5} M. If the concentration of **3** in these solvents is further increased, we witness the formation of the D-band in UV/vis spectroscopy that is indicative for the generation of centrosymmetric units of aggregated merocyanine chromophores.[26] Because each molecule of dye **3** contains two merocyanine dyes, a chain growth is expected at this transition with increasing concentration. However, only short oligomeric chains are given in DCM or THF up to a concentration of 10^{-4} M that is the limiting concentration for our UV/vis instrument for these strongly absorbing chromophores. The change to the less polar solvent TCE leads to a situation where the thermodynamically equilibrated solutions exhibit most dyes in a D-aggregated form at a concentration of 10^{-5} M. For the D-aggregated state, we assume the presence of polymeric chains with a chain length distribution and the population of several conformations (i.e., statistical coil formation) similar to those of common polymeric compounds. However, the presence of cyclic oligomers cannot be ruled out.[34]

Owing to the rigidity of the bis(merocyanine) building blocks (only four rotable σ-bonds at the methylene bridges) and the highly directional aggregation of chromophores into dimeric units, these polymeric chains exhibit only a limited number of conformational states. According to molecular modeling, a randomly oriented chain can easily reorganize (i.e., with little or no energetic penalty) into a well-defined helical polymer with a pitch of ~5 nm as suggested in Figure 14B. Note that both possible helices are equally populated as no CD effects could be observed for MCH solutions of **3**. Based on molecular modeling[38] and experimental support from our AFM and X-ray data (discussed later), six of these supramolecular polymeric chains are able to assemble to give a tubular dye aggregate (Figure 14C) that is jacketed by the aliphatic chains of the tris(*n*-dodecyloxy)xylylene substituents. For such an assembly, each merocyanine dye is aggregated to a closest dye neighbor ($d \approx$ 3.5 Å) and to a second slightly more distant dye neighbor ($d \approx$ 4 Å). On both π-faces, an antiparallel orientation for the neighboring dye is possible (situation of optimal electrostatic energy) taking into account the geometrical features of the molecule, i.e., the van der Waals volume. According to our studies, this is the situation for the H-aggregated state which is the thermodynamically stable one in low polarity aliphatic environments.

Interestingly, similar structural features of a close and a more distant neighbor have been observed in two crystal structures of related merocyanine dyes in our recent work.[26] In the absence of structural restrictions as imposed by the rigid xylylene linkage of two chromophores in dye **3**, simple antiparallel stacking leading to a one-dimensional aggregate occurred in these examples. In the given situation, however, a cylindrical assembly is formed that contains twelve dyes in a cross section of the rod-shaped fiber (Figure 14C) according to our model. The blue-shifted H-aggregate band confirms that the excitons are delocalized over more than two dyes, but an exact number is not derivable from the currently available data. The close structural resemblance to the bacteriochlorophyll c based chlorosome rod elements of the light-harvesting system of green bacteria[2] and recently investigated porphyrine[39,40] and cyanine dye *J*-aggregates[41] are, however, noteworthy.[42] Both of these examples bear highly delocalized excitonic states due to close contacts of highly polarizable dyes, a feature which is shared by our system.

According to our UV/vis studies, fibers of dyes **3** exhibit fairly high stability in solvents of intermediate polarity like TCE, and their disassembly requires long time or elevated temperatures owing to a significant activation energy barrier. Such highly stable superstructures are in the meanwhile more often observed in self-assembling systems if several receptor units interact in a cooperative way to yield a higher order supramolecular object of enhanced stability. An especially intriguing example for the formation of a chiral double rosette assembly from achiral building blocks was recently shown by Reinhoudt and coworkers.[43] In this example, the kinetic stability was used to exchange chiral for achiral building blocks without destroying the macroscopic chirality of the double rosette assembly that is held together by 36 hydrogen bonds and $\pi-\pi$-stacking interactions.

Based on the structural model in Figure 14C, the kinetic stabilization of the H-aggregated rod elements of **3** is easily explained by strong dipolar interactions of each dye to two neighbors, one on the top and one on the bottom face of the π-conjugated system. The high stability of this assembly and the rigid rod-shaped structure are also supported by our AFM as well as our viscosity measurements that prove high intrinsic viscosities over the whole accessible concentration range from 5×10^{-4} to 5×10^{-3} M in MCH. So far, such high viscosity could be only observed for a few supramolecular polymers that exhibit very high binding strength due to multiple hydrogen bonding or metal−ligand coordination interactions.[12] In our system, the binding strength is the result of two binding events on both faces of the π-surface of the dyes. For the first dye−dye interaction, we can safely assume a Gibbs interaction enthalpy of about 45 kJ/mol (corresponding to a dimerization constant of 10^8 M^{-1}) according to our earlier studies with dyes **2**.[26] The second binding event contributes another stabilization energy of unknown magnitude.

Analyzation of the viscosity−concentration curves in terms of reversible polymerization models was attempted,[20] assuming the presence of statistical coils made up from individual polymeric chains. Though numerical fits yielded plausible values of the association constant ($K_{AA} \approx 10^8$ M^{-1}), the calculated Staudinger−Mark−Houwink exponents were very small ($a \approx$ 0.1−0.2). In contradiction to experimental evidence, such low values would indicate the presence of globular superstructures. Furthermore, the derived linearized plots systematically failed with solutions of pure **3** or low contents of monofunctional dye **4**. It was concluded that this failure was caused by the presence of (i) "multichain" superstructures and (ii) cooperative effects that were not taken into account by the simple "statistical polymer" theory.

(38) Calculated with MM+ force field as implemented in HyperChem 6.0, Hypercube Inc. USA, 2000.
(39) Balaban, T. S.; Bhise, A. D.; Fischer, M.; Linke-Schaetzel, M.; Roussel, C.; Vanthuyne, N. *Angew. Chem., Int. Ed.* **2003**, *42*, 2140−2144.
(40) (a) Kano, K.; Fukuda, K.; Wakami, H.; Nishiyabu, R.; Pasternack, R. F. *J. Am. Chem. Soc.* **2000**, *122*, 7494−7502. (b) Collings, P. J.; Gibbs, E. J.; Starr, T. E.; Vafek, O.; Yee, C.; Pomerance, L. A.; Pasternack, R. F. *J. Phys. Chem. B* **1999**, *103*, 8474−8481.
(41) (a) Pawlik, A.; Kirstein, S.; De Rossi, U.; Dähne, S. *J. Phys. Chem. B* **1997**, *101*, 5646−5651. (b) Berlepsch, H. von; Böttcher, C.; Dähne, L. *J. Phys. Chem. B* **2000**, *104*, 8792−8799.
(42) In contrast to the aggregates of cationic cyanine dyes, refs 8, 9, 41, however, self-organization of dye **3** is driven by well-defined dipolar interactions and takes place in organic solvents.
(43) Prins, L. J.; Verhage, J. J.; de Jong, F.; Timmerman, P.; Reinhoudt, D. N. *Chem.−Eur. J.* **2002**, *8*, 2302−2313.

Table 2. Evaluation of Viscosity Data Obtained for Solutions of **3** and **3/4** Mixtures in Methylcyclohexane at 30 °C[a]

X_4	$[\eta]$ [mL g^{-1}]	α	$\langle X_\eta \rangle$	$\langle M_\eta \rangle$[g mol^{-1}]
0	644	140	4000	6.0×10^6
0.1	307	93	2600	3.9×10^6
0.2	174	67	1900	2.8×10^6

[a] X_4 = molar fraction of monofunctional dye **4** added to the bifunctional dye **3**, $[\eta]$ = intrinsic viscosity, α = aspect ratio, $\langle X_\eta \rangle$ = viscosity average degree of polymerization, $\langle M_\eta \rangle$ = viscosity average molecular weight.

Based on the results of the X-ray, AFM, and electron microscopy investigations, the presence of rigid rodlike superstructures was unambiguously confirmed. In this case, the intrinsic viscosities $[\eta]$ of the methylcyclohexane solutions of **3** can approximately be related to the aspect ratio $\alpha = L/d$ of the rods and allows estimating the degree of polymerization $\langle X_\eta \rangle$:[44]

$$[\eta] = \frac{8}{(45 + a)} \cdot \frac{1}{\rho} \cdot \frac{\alpha^2}{\ln(\alpha + K)} \tag{2}$$

$$\langle X_\eta \rangle = \frac{\pi}{4} \cdot \frac{N_A \cdot \rho \cdot d^3 \cdot \alpha}{M_0} \tag{3}$$

($[\eta]$ = Staudinger index, ρ = density of the rod, $\alpha = L/d$ = aspect ratio of the rod, L = rod length, d = rod diameter, $\langle X_\eta \rangle$ = viscosity average degree of polymerization, M_0 = molecular weight of the monomer. Kirkwood − Riseman theory: $a = K = 0$. Doi−Edwards theory: $a = 3$, $K = 2\ln(2) - {}^7/_3$).

The density of the rods was calculated from the molecules' volume ($v_m = 2.3$ nm^3) and its molecular weight to yield $\rho = 1.1 \pm 0.1$ g cm^{-3}; the rod diameter was taken from the X-ray data to be $d = 4.3$ nm. The evaluation of the viscosity data according to this model is summarized in Table 2. Calculation of the aspect ratio according to eq 2 yielded a value of $L/d = 140$ for pure **3**. If the rod diameter was assumed to amount to 4.3 nm, the degree of polymerization was 4000 units of **3**, corresponding to a molecular weight of 6×10^6 g mol^{-1}.

It is also in accordance with the supramolecular polymerization model that the viscosity of MCH solutions of bis(merocyanine) dye **3** is reduced upon addition of monotopic merocyanine dye **4**. Similar "chain stopper" experiments have been performed for hydrogen-bonded polymers and demonstrated their reversible nature. Compared to these examples, we note that the decrease in viscosity per equivalent added stopper molecule is not as pronounced for our system. Based on our structural model in Figure 14C, this is easily understood because the incorporation of the "chain stoppers", monofunctional molecules, does not benefit from the cooperative enhancement of the interaction energy. In addition, we have to consider that the fiber is formed by several intertwined polymeric strands. Thus, incorporation of a few monofunctional dyes into the rod aggregates will not necessarily destroy the whole fiber as long as the neighboring polymeric chains remain intact. However, the addition of chain stoppers to **3** decreased the aspect ratio of the rods. The addition of 20 mol % of **4** reduced α by a factor of 2. The same holds true for the degree of polymerization provided the rod diameter was not altered on addition of chain stopper molecules.

A second observation from our viscosity measurements was the structural growth to the next level of hierarchy at a concentration exceeding 2×10^{-3} M where the slope of the reduced viscosity showed a significant increase. This viscosity increase is attributed to the onset of three-dimensional network-like branching, i.e., formation of cross-linked microgel clusters. Progress of this process at increasing concentration is further supported by gelation when the concentration approaches 10^{-2} M. From the model of the fiber (Figure 14C), it is easy to relate this network and gel formation to junction zones that form by interpenetration of the dodecycloxy chains that cover each fiber's periphery. The inclination toward formation of such junction zones is clearly established from our AFM study (Figure 11). In contrast to the former strong electrostatic interactions between the dyes, this interaction between the alkyl chains is rather weak in accordance with the rheology measurements. The weak nature of the van der Waals interaction between alkyl chains fully agrees with the low stress resistance of the storage modulus measured from the organogels. Hence, the cross-linking points in the gel are induced by entanglement rather than by crystalline microdomains. The presence of rod aggregates was also confirmed by cryo-TEM and AFM. Whereas the former method provided only an upper limit of 10−15 nm for the rod diameter owing to the platinum shadowing technique, excellent lateral and vertical resolution was achieved by AFM confirming the size (diameter of 3.4−4.8 nm), shape (circular cross-section), and the considerable length (high aspect ratio) and rigidity of the rod aggregates in full accordance with the model in Figure 14C.

If the concentration is further increased, more and more of these rods align in a parallel fashion (cf. AFM study, Figure 11) giving rise to lyotropic liquid-crystalline phases with birefringent textures. After the solvent is completely evaporated, the texture shown in Figure 12 is obtained and a hexagonal columnar order is found by X-ray diffraction analysis. It is of major importance for the structural model of Figure 14D that the lattice constant for the hexagonal phase is in excellent agreement with the calculated rod diameter from molecular modeling. From the X-ray data (Table 1), the intercolumnar distance is 4.34 nm which compares to a rod diameter of 2.5 nm for the rigid inner core of the π-systems and a rod diameter of 5.1 nm including the fully extended alkyl chains of the trialkoxyxylylene side chains. The latter are, however, expected to interpenetrate into neighboring columns which is the driving force for the formation of gels. Therefore, the intercolumnar distance of 4.34 nm perfectly matches our expectations based on the model from Figure 14C and our AFM results. Furthermore, the model is also supported by density measurements (see Experimental Section). According to Figure 14C, about five molecules are included in a pitch of the helical chain and, therefore, there are 30 molecules in the column within this distance. This number is in agreement with the number 32 ± 2 molecules calculated from the volume of a 5 nm long and 4.34 nm diameter column divided by a partial molecular volume of 2.3 ± 0.1 nm^3 per molecule. Assuming a length of the fiber of about 2 μm as suggested by AFM and TEM, we can estimate an aggregation number larger than 1.2×10^4 for these rod-shaped H-aggregates. Note that these values roughly correspond to the estimations from viscosity data ($L \approx 0.7$ μm, $\langle X_\eta \rangle = 5700$).

(44) Yamakawa, A. *Modern Theory of Polymer Solutions*; Harper and Row: New York, 1971.

Conclusion

Supramolecular dye polymers exhibiting viscous and viscoelastic properties could be realized by self-organization of bis(merocyanine) **3** in nonpolar solvents. Through electrostatic interaction between these highly dipolar dyes, chain growth polymerization and further hierarchical growth to rod-shaped dye assemblies resulted. Based on structural data (AFM, TEM, and X-ray diffraction) and supported by optical spectroscopy (narrow H-aggregate band in the UV/vis), viscosity data, and molecular modeling, a structural model could be derived showing the dyes aggregated in a circular fashion to give rod-shaped fibers with a diameter of 4.3−4.8 nm and several micron length. The formation of these fibers can be understood in terms of a second process of self-organization by intertwining of six individual supramolecular polymeric chains that are helically preorganized. For such an assembly, all alkyl groups of the tris(*n*-dodecyloxy)xylylene substituents point to the outside and provide solubility in low-polarity environments. Upon increasing concentration in aliphatic solvents, the alkyl chains at the periphery entangle leading to a significant increase of viscosity and even viscoelastic properties. At even higher concentration, gel formation and lyotropic mesophases are observed. Finally, upon evaporation of the solvent, films are formed that exhibit birefringent patterns due to the hexagonal columnar ordering of the rod-type aggregates.

Experimental Section

Methods. A. UV/vis Absorption Spectra were recorded in spectroscopic grade solvents without further purification using matched silica cells. The spectral bandwidth and the scan speed used were 1.0 and 120 nm/min. Dimer formation studies of dye **4** and aggregation studies of dye **3** were carried out in 1.0 cm cells. The stock solutions of each compound were prepared accurately, and dilutions of these stocks were used for absorption measurements over a concentration range taking into account solubility and absorbance. In the case of temperature-dependent studies, the temperature was controlled with a deviation of ±0.1 °C by circulating a mixture of water/ethyleneglycol = 1:1 from a thermoregulator.

B. Viscosity Measurements. Solution viscosities were measured at 30 °C with a capillary viscometer using an automated viscosity measuring unit to obtain reproducible run times. The effective capillary diameters were 0.47 mm, 0.63 mm, and 1.13 mm. The setup was mounted in a thermostat, which was controlled by circulating a mixture of water/ethyleneglycol = 1:1. The measurements were run from concentrated to diluted solutions. Dilution was achieved by using an automated Titronic device. The reduced viscosity (η_{red}) was obtained from eq 4:

$$\eta_{\mathrm{red}} = \frac{t_{\mathrm{dye}} - t_{\mathrm{sol}}}{t_{\mathrm{sol}}} \cdot \frac{1}{c_{\mathrm{dye}}} \tag{4}$$

where t_{dye} and t_{sol} denote the run time of the dye solution and the pure solvent, respectively, while c_{dye} represents the concentration of the dye solution in g of dye L^{-1} of solvent.

C. Gelation Tests. A typical procedure for qualitative gelation testing was as follows: In a test tube, dye **3** was mixed with appropriate amounts of solvent and the mixture was heated until the solid dissolved. The resulting clear solution was cooled to 20 °C and annealed for more than 12 h at this temperature. When the test tube could be inverted without change of shape of its content, it was identified as a gel.

D. Rheology Measurements. The measurements were performed using a stress controlled Dynamic Stress Rheometer, equipped with a Bob−Couette geometry at 25 °C. The diameter of the bob was 32.5 mm; the width of the gap was 1.5 mm. A hot solution of dye **3** in *n*-octane was introduced in the shearing gap of the rheometer and was allowed to equilibrate for 1 h. Subsequently it was submitted to a frequency sweep or stress sweep experiment. To minimize solvent evaporation, the measuring cell was covered by a lid containing an octane-filled fleece.

E. Density Measurement. The density of dye **3** in dilute methylcyclohexane solution was determined by a density meter at 25 ± 0.1 °C, regulated by a thermostat. The solutions used for the measurement were prepared by diluting a 0.6896 wt % stock solution. The partial molecular volume was calculated according to eq 5.[45]

$$\frac{1}{\rho} = \frac{1}{\rho^*} + \left(\frac{V_{\mathrm{dye}}^*}{M_{\mathrm{dye}}} - \frac{1}{\rho^*}\right) \tag{5}$$

where ρ is the density of the dye solution, ρ^* is the density of methylcyclohexane (765.0 kg m^{-3} at 25 °C), V_{dye}^* is the partial mole volume of dye **3**, M_{dye} is the molecular mass (M_{dye} = 1498.29 g mol^{-1} for dye **3**), and w_{dye} is the weight fraction of dye **3** in solution. By linear fitting of $1/\rho$ vs w_{dye}, a partial mole volume of 1.395×10^{-3} m^3 mol^{-1} resulted with a deviation of 4%, corresponding to a partial molecular volume of $\nu_{dye} = 2.3 \pm 0.1$ nm^3.

F. Electron Microscopy. Samples were frozen in liquid nitrogen and cryo-fractured in a "freeze etching device" at a temperature of −150 °C and coated with 2 nm of platinum at an angle of 45° and 10 nm of carbon perpendicularly. The replicas were cleaned in chloroform and imaged in a electron microscope at an accelerating voltage of 80 kV.

G. AFM Measurements were performed under ambient conditions using a commercial scanning probe microscope operating in tapping mode. Silicon cantilevers with a resonance frequency of ∼300 kHz were used. The 512 × 512 pixel images were collected at a rate of 2 scan lines per second. Solutions of dye **3** in MCH (10^{-4} M) were spin-coated onto an HOPG under 5000 rpm.

H. Polarizing Optical Microscopy. A sample was prepared by evaporation of a drop of a 1.0 g L^{-1} solution of dye **3** in methylcyclohexane on a glass slide. Then the optical textures at crossed polarizers were recorded with a polarization microscope at room temperature.

I. Wide- and Small-Angle X-ray Scattering (WAXS and SAXS). A thick film (0.5−1.0 mm) was prepared from multistep evaporation of a 5.0 g L^{-1} solution of dye **3** in methylcyclohexane on aluminum foil. The X-ray diffractogram were recorded at room temperature using Ni-filtered $Cu_{k\alpha}$ radiation on a powder diffractometer for WAXS and a home-build setup for SAXS.

J. NMR Spectra were recorded at room temperature in $CDCl_3$ or in a mixture of CD_2Cl_2/CD_3OD = 80:20. CD_2Cl_2 was chosen as solvent to avoid any superposing of the solvent peak with substance peaks and CD_3OD was added to increase the permittivity. This gave more defined spectra due to reduced aggregation. Chemical shifts are given in ppm downfield from TMS, coupling constants are given in Hertz.

Materials. All solvents were obtained from commercial sources and purified and dried according to standard procedures.[46] 1,2,3-Tris(*n*-dodecyloxy)benzene **5**[47] and 1-dodecyl-4-methyl-2,6-dioxo-1,2,3,6-tetrahydropyridine-3-carbonitrile **9**[26] were synthesized according to literature procedures.

A. 1,3-Bis(bromomethyl)-4,5,6-tris(*n*-dodecan-1-yloxy)benzene (6). To a suspension of 1,2,3-trisdodecyloxybenzene **5** (27.5 g, 43.0 mmol) and paraformaldehyde (2.64 g, 87.8 mmol) in acetic acid (150 mL) was added HBr (17 mL, 33 wt % in acetic acid) all at once. This mixture was then heated to 70 °C for 120 h. The resulting suspension was poured into water (1 L). The aqueous layer was extracted with 3

(45) Wortmann, R.; Elich, K.; Lebus, S.; Liptay, W.; Borowicz, P.; Grabowska, A. *J. Phy. Chem.* **1992**, *96*, 9724−9730.
(46) Perrin, D. D.; Armarego, W. L. F.; Perrin, D. R. *Purification of Laboratory Chemicals*; Pergamon Press: Oxford, 1980.
(47) Percec, V.; Ahn, C.-H.; Bera, T. K.; Ungar, G.; Yeardley, D. J. P. *Chem.−Eur. J.* **1999**, *5*, 1070−1083.

× 500 mL of ether. The combined organic phase was washed with water and dried over Na_2SO_4. Solvent evaporation afforded 34.6 g of product (98% yield). ^{1}H NMR (400 MHz, $CDCl_3$) δ 7.10 (s, 1H, H-ph), 4.49 (s, 4H, $BrCH_2$), 4.13 (t, J = 6.8 Hz, 2H, OCH_2), 3.95 (t, J = 6.7 Hz, 4H, OCH_2), 1.78 (m, 6H, CH_2), 1.52−1.24 (m, 54H, CH_2), 0.88 (t, J = 6.8 Hz, 9H, CH_3). HRMS (EI, 70 eV): $[M - Br]^+$ 735.5290 (calcd 735.5291). Anal. Calcd for $C_{44}H_{80}Br_2O_3$ (816.91): C, 64.69; H, 9.87. Found: C, 65.18; H, 9.72.

1,1′-[4,5,6-Tris(*n*-dodecan-1-yloxy)-1,3-phenylenebis(methylene)] Bis(4-methylpyridinium)dibromide (7). The foregoing bis(bromomethyl)benzene **6** (52.8 g, 64.6 mmol) and 4-methylpyridine (22.6 g, 242 mmol) in 500 mL of acetonitrile were refluxed for 31 h. The solvent was evaporated under reduced pressure, and the residue was recrystallized from acetone to give 48.3 g of dipyridinium salt **7** (75% yield); mp 181−182 °C; ^{1}H NMR (400 MHz, $CDCl_3$) δ 9.33 (d, J = 5.3 Hz, 4H, H-pyridine), 8.01 (s, 1H, H-ph), 7.90 (d, J = 5.9 Hz, 4H, H-pyridine), 5.88 (s, 4H, NCH_2), 4.16 (t, J = 6.8 Hz, 4H, OCH_2), 3.90 (t, J = 5.7 Hz, 2H, OCH_2), 2.65 (s, 6H, CH_3), 1.73 (m, 6H, CH_2), 1.48−1.20 (m, 54H, CH_2), 0.88 (t, J = 6.8 Hz, 9H, CH_3). Anal. Calcd for $C_{56}H_{94}N_2O_3Br_2$ (1003.19): C, 66.05; H, 9.44; N, 2.79. Found: C, 66.08; H, 9.33; N, 2.71.

1-[2,3,4-Tris(*n*-dodecan-1-yloxy)benzyl]-4-methylpyridinium Bromide (8). To a suspension of trisdodecyloxybenzene **5** (1.26 g, 2.0 mmol) and paraformaldehyde (0.06 g, 2.0 mmol) in acetic acid (5 mL) was added HBr (0.355 mL, 33 wt % in acetic acid) all at once. This mixture was then heated to 70 °C for 4 h and distilled under reduced pressure to dryness. 4-Methylpyridine (0.19 g, 2.0 mmol) and acetonitrile (10 mL) were added, and the mixture was refluxed for 24 h. The solvent was evaporated under reduced pressure, and the crude product was recrystallized from acetone to give 0.52 g of pyridinium salt **8** (32% yield). ^{1}H NMR (400 MHz, $CDCl_3$) δ 9.24 (d, J = 6.6 Hz, 2H, H-pyridine), 7.72 (d, J = 6.3 Hz, 2H, H-pyridine), 7.63 (d, J = 8.6 Hz, 1H, H-ph), 6.67 (d, J = 8.7 Hz, 1H, H-ph), 5.99 (s, 2H, NCH_2), 4.12 (t, J = 7.1 Hz, 2H, OCH_2), 3.94 (m, 4H, OCH_2), 2.62 (s, 3H, CH_3), 1.73 (m, 6H, CH_2), 1.26 (m, 54H, CH_2), 0.88 (m, 9H, CH_3).

Bis(merocyanine) Dye 3. Dodecylpyridone **9** (0.96 g, 3 mmol) and *N*,*N*′-diphenylformamidine (0.59 g, 3 mmol) in Ac_2O (5 mL) were stirred at room temperature for about 15 min until the mixture solidified. Then the mixture was heated at 90 °C for an additional 30 min to complete the formylation reaction. After cooling to room temperature, bis(pyridinium) salt **7** (1.00 g, 1 mmol) and KOAc (0.29 g, 3 mmol) were added, and the mixture was heated at 100 °C for 20 h. The resulting solution was cooled to room temperature, and a red solid was precipitated by adding 5 mL of acetone. The filtered solid was purified by flash column chromatography using silica gel and CH_2Cl_2/CH_3OH = 94:6 as eluent. Precipitation from dichloromethane/acetone gave 0.72 g of dye **3** (48% yield). Mp 288−289 °C (dec); ^{1}H NMR (400 MHz, H−H-COSY, CD_2Cl_2/CD_3OD) δ 8.06 (d, J = 7.0 Hz, 4H, H-pyridine), 7.70 (d, J = 14.9 Hz, 2H, H-methine), 7.58 (d, J = 15.0 Hz, 2H, H-methine), 7.42 (s, 1H, H-ph) 7.41 (d, J = 7.3 Hz, 4H, H-pyridine), 5.34 (s, 4H, NCH_2), 4.12 (t, J = 6.9 Hz, 4H, OCH_2), 3.93 (m, 6H, NCH_2, OCH_2), 2.35 (s, 6H, CH_3), 1.75 (m, 6H, CH_2), 1.56 (m, 4H, CH_2), 1.50−1.10 (m, 90H, CH_2), 0.87 (m, 15H, CH_3). MS (Fab, 3-nba): 1521 $[M + Na]^+$. UV/vis (CH_2Cl_2 at 10^{-6} M): λ_{max} = 566 nm (ϵ_{max} 223 000 L mol^{-1}cm^{-1}). Anal. Calcd for $C_{96}H_{148}N_6O_7$ (1498.3): C, 76.96; H, 9.96; N, 5.61. Found: C, 76.56; H, 10.20; N, 5.52.

Merocyanine Dye 4. Dodecylpyridone **9** (0.22 g, 0.69 mmol) and *N*,*N*′-diphenylformamidine (0.14 g, 0.69 mmol) in Ac_2O (3 mL) were stirred at room temperature for 15 min until the mixture solidified. Then the mixture was heated at 90 °C for 15 min to complete the reaction. After cooling to room temperature, pyridinium salt **8** (0.52 g, 0.64 mmol) and KOAc (0.1 g, 1 mmol) were added, and the mixture was heated at 100 °C for 20 h. The resulting solution was evaporated in vacuo and purified by column chromatography using silica gel and CH_2Cl_2/CH_3OH = 96:4 as eluent. Precipitation from dichloromethane/acetone gave 0.53 g of dye **4** (77% yield). Mp 124−125 °C; ^{1}H NMR (400 MHz, $CDCl_3$) δ 7.72 (d, J = 15.3 Hz, 1H, H-methine), 7.69 (d, J = 7.7 Hz, 2H, H-pyridine), 7.41 (d, J = 14.7 Hz, 1H, H-methine), 7.18 (d, J = 6.8 Hz, 1H, H-ph), 7.13 (d, J = 6.7 Hz, 2H, H-pyridine), 6.67 (d, J = 8.5 Hz, 1H, H-ph), 5.28 (s, 2H, NCH_2), 3.99 (m, 6H, OCH_2), 3.91 (t, J = 6.6 Hz, 2H, NCH_2), 2.22 (s, 3H, CH_3), 1.83 (t, J = 7.3 Hz, 2H, CH_2), 1.72 (t, J = 7.3 Hz, 2H, CH_2), 1.63 (m, 6H, CH_2), 1.44 (m, 70H, CH_2), 0.87 (m, 12H, CH_3). UV/vis (CH_2Cl_2 at 10^{-5} M): λ_{max} = 550 nm (ϵ_{max} 117 000 L mol^{-1} cm^{-1}). Anal. Calcd for $C_{69}H_{113}N_3O_5$ (1064.7): C, 77.84; H, 10.70; N, 3.95. Found: C, 77.78; H, 10.49; N, 3.90.

Acknowledgment. This work was supported by the Deutsche Forschungsgemeinschaft, DFG (Research Grant Wu 317/1-3). We are grateful to Prof. Paul Walther for his help on electron microscopy performed at the "Central Electron Microscopy Unit" of the University of Ulm, to Prof. Rüdiger Wortmann (Universität Kaiserslautern) for his help on density measurements, and to Dr. Bernd Heise (Department of Experimental Physics, Ulm) for carrying out the SAXS measurements.

Supporting Information Available: Additional UV/vis absorption spectra of **3** and **4**. This material is available free of charge via the Internet at http://pubs.acs.org.

JA0496367